

# A Stochastic Compound Failure Model for Testing Resilience of Autonomous Fixed-Wing Aircraft I: Formulation and Simulation

Thelonious Cooper and Sai Ravela  
Earth Signals and Systems Group  
Massachusetts Institute of Technology  
77 Massachusetts Avenue, Cambridge, MA 02139

This paper presents a simulation process to dynamically emulate the effects of certain adversarial flight conditions on fixed-wing, autonomous aircraft system actuators. We implement a PX4 Autopilot flight stack module that replaces the generated attitude control inputs with perturbed inputs to the plane’s actuator mixer. The perturbed inputs rely on a Markov chain to model failure states that emulate adversarial (failing) actuator flight conditions. Simulated flight failures on a fixed-wing autonomous aircraft test the controller response to a stochastic failure sequence on a range of turning radii. Statistical measures between the differences between unaffected and perturbed flight paths provides analyses, indicating that a well-tuned PID controller remains competitive in the cascading, compound, transient failure regime.

## I. INTRODUCTION

Despite their inadequacies in adverse conditions, low-cost fixed-wing Uncrewed/autonomous Aircraft Systems (UAS) are immensely interested in environmental research. Where satellite imagery is too infrequent, strapping sensors to an inexpensive UAS and flying them is attractive for collecting data. In these missions, aircraft damage and payload losses are substantial when parts fail, even when the UAS itself is repairable. For missions such as flying into a volcanic plume or shallow cumuli [30, 32], errant ash or soot jamming a servo could mean loss of data and thousands of dollars.

In such flights, numerous things can go wrong. Electrical or communication failures induced by the environment, low-quality servos and cabling, poor thermal management, poorly strapped payload, and even mismatched wing surfaces are all culprits. In many situations, the failures are not immediately catastrophic and permanent but incipient transient that, if left unattended, become cascading compound failures, followed by total failure and permanent loss as too many things go wrong. In the real world, cascading failures often turns initial confusion to utter panic in the field that, more than anything else, leads to a crash. In other situations, a few parts may completely fail, still rendering the aircraft flyable using redundant control surfaces or sensors. In still different cases, there may be some degraded performance.

Improving autopilot resilience, that is, handling and recovering from developing transient in-flight failures would tremendously advance operating low-cost UAS for adverse environments. However, this is easier said than done. Hierarchical PID controllers are the heart of most modern hobby/environmental research uncrewed/autonomous aircraft autopilots. Stock controllers [25] are generally well-tuned, but conventional wisdom is that finely-tuned autopilots are not responsive to incessant hiccups. We do not expect stock hierarchical PID controllers to adapt quickly to changing vehicle dynamics, and some adaptive control appears to be needed.

One approach is to model the aircraft dynamics carefully under various failure conditions, detect them in flight to trigger an appropriate control law. This might take the form of model predictive control, and include online model parameter tuning and coupling with PID control to handle model imperfections. However, hybrid approaches such as these are likely to be very expensive. Adaptive control, if we are to incorporate it, must be low-cost. In this context, exciting new developments in Retrospective Cost Adaptive Control (RCAC) [13–15, 24] suggest that PID gains are tunable in a data-driven manner by optimizing a performance index on a retrospective performance variable. The RCAC solution recursively updates gains that are easy to implement on the typically low-cost hardware that stock autopilots such as PX4 [6, 25] used in this research.

Previously, we implemented RCAC for quadrotor [14, 15, 33] and fixed-wing aircraft [24] in the PX4 environment (PX4 v1.10) [6, 25] with Holybro Pixhawk (FMUv5) [4] hardware, and have tested them in software-in-the-loop, hardware-in-the-loop, and assisted flight configurations (see Figure 1. In these tests, we flew the aircraft in *clean* and *adversarial* (simulated failure) conditions, where cutting an actuator simulates failure. These configurations tested single step failure injection. Based on our flight testing experience with fixed-wing aircraft, we posit that in many real-world cases, cascading, compounding intermittent failures that, left unresolved, become total failures, are common.

In this storyline, we start with a well-tuned aircraft. That is, we are generally satisfied with the autopilot in clean conditions. We augment this autopilot with an adaptive controller (RCAC) so that when transient failures appear, typically milli-seconds to seconds long, the system shows some skill at adapting and maintaining performance. That is a much more demanding scenario, but essential to test before operational use.

Systematic approaches to testing cascading and compounding stochastic failures are not readily available for PX4-like stock autopilots in small-UAS settings. Here,

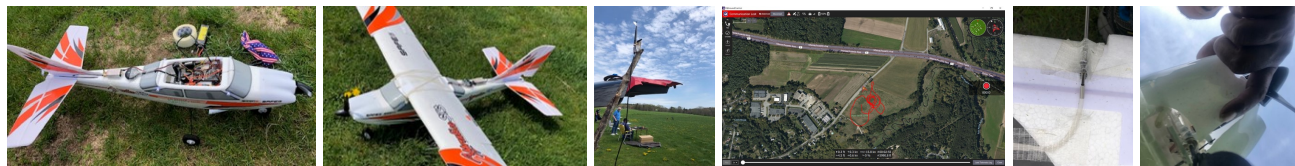


Figure 1: The Earth Signals and Systems group flies multiple aircraft for environmental applications, testing new control laws. Here, we show snapshots of a flight test with RCAC [24]. From left to right, the Pixhawk autopilot mount, the aircraft, ground station, flight path, pitot tube assembly, and broken nose wheel. Such conditions as taped pitot tube and broken assemblies are common in hobby flying.

we develop a stochastic model wherein a stationary Markov chain simulates failure. It transitions the aircraft from a safe state (the clean configuration) to various degrees of simulated failure conditions, locking and releasing a combination of actuators at any given time. In this first attempt, the Markov transition matrix only loosely corresponds to observations from extensive prior flight experience (for example, see Figure 1) and use a Hardware-in-the-Loop (HITL) environment to test simulated failures and trajectories for the fixed-wing aircraft.

The central hypothesis tested checks whether adding an adaptive control component offers significant advantages over well-tuned stock autopilots in the transient, cascading, and compound failure regime. Our results indicate that with specific hyper-parameter tuning, RCAC handles step changes to flight configurations deftly. Previous work [24, 33] shows that mixing its control inputs with the stock PX4 autopilot [25] has a particular advantage for compensating poorly calibrated PID parameters. We find no specific benefit in the transient failure regime at typical timescales of interest. In a sense, the adaptations highly tune the aircraft to specific regimes, making transitions to other regimes in a stream of failures difficult. It is possible that the issue could be addressed by additional possibly dynamic hyper-parameter tuning but no clear strategies emerge as of this writing to handle failures at different rates.

The remainder of this paper is as follows. Section II describes related work. Section III describes the stock PID (PX4 v1.10) [25] controller and RCAC [24], and Section IV describes flight-path generation, Markov failure model, and comparison measures. Section V discusses implementation details for the Holybro Pixhawk (FMUv5), and a Discussion and Conclusions follow.

## II. RELATED WORK

Several adaptive control techniques for controlling fixed-wing aircraft [26] such as sliding mode [12, 37], backstepping-based nonlinear controller [18], and MRAC-based control augmentation [36]. Although approaches such as ensemble control [34] on embedded GPUs are advancing, computationally expensive detailed models are still needed. We use RCAC, which is low cost and uses the past measured data and control inputs to

recursively estimate controller gains [14, 24, 29, 33]. Extension to digital PID control [21], multicopter autopilot [14, 33] is available with an implementation for the PX4 Pixhawk platform. In previous work [24], RCAC was used to compensate for singleton actuator faults in both calibrated and degraded PX4 conditions [24], which we refer the reader to as the primary reference for details. Here, we use this framework to test performance over a stream of the transient compound, cascaded actuator faults.

Prochazka et al. [28] develop a HITL demonstrator for validating fault-tolerant control methods for a hybrid UAV, where they simulate actuator failure and subsequent reconfiguration by a fault-tolerant flight control law. Jha et al. [20] develop a fault injector for autonomous vehicles, including data, hardware, timing, and machine learning subsystem components. Wen et al. [35] describe a fault simulator for UAS that includes sensor and actuator failures with human-in-the-loop flying. Gong et al. [16] argue that prior data is limited and develop a fault injector for UAS process health monitoring. This work produces a stochastic Markov model for singleton, compound, and cascading actuator failures. Although unimplemented here, flight data can train the pre-specified transition probabilities.

## III. CONTROLLERS

Our synthetic experiments test two flight controllers. The first is the stock PX4 autopilot based on hierarchical PID [25], and the second is RCAC [24]. This section briefly discusses each controller. A GitHub page [10] contains the implementation of our work in the PX4 environment.

### A. PX4 PID Controllers for Fixed Wing Aircraft

The PX4 autopilot [6] receives position setpoints from a Ground Controller (e.g., QGroundControl, Mission Planner) and controls the fixed-wing aircraft with two nested-loop cascaded controllers. A position controller operates the outer loop for longitudinal and lateral motion control, and an attitude controller operates the inner loop. The position controller’s longitudinal control sec-

tion sets the thrust ( $T_s$ ) and pitch ( $\theta_s$ ) set points, and the lateral control section sets the roll ( $\phi_s$ ) set point. The attitude controller cascades two controllers. The first controller sets pitch ( $\dot{\theta}_s$ ) and roll ( $\dot{\phi}_s$ ) rates proportionately to roll and pitch errors (computing the yaw rate is algebraic). The second controller employs a feedforward and Proportional-Integral (PI) control law to set the angular acceleration. Control allocation methods then set actuator deflections using the angular acceleration set points.

Thus, the position controller takes the True airspeed ( $V_{tas,s}$ ), attitude, and position setpoints and the corresponding measurements of true airspeed ( $V_{tas}$ ), attitude, and position to set the thrust  $T_s$ , roll  $\phi_s$ , and pitch  $\theta_s$  demands. Its longitudinal control section employs a Total Energy Control System (TECS) [7, 9, 11, 23], using a different guidance law [27] for lateral control.

The attitude controller's proportion control law uses gains  $k_\theta$  and  $k_\phi$  to produce rate setpoints:

$$\begin{aligned}\dot{\theta}_s &= k_\theta(\theta_s - \theta_m), \\ \dot{\phi}_s &= k_\phi(\phi_s - \phi_m).\end{aligned}\quad (1)$$

The yaw rate setpoint ( $\dot{\psi}_s$ ) uses the true airspeed  $V_{tas}$  and attitude to set develop a coordinated turn:

$$\dot{\psi}_s = \frac{g \tan \phi_s \cos \theta_s}{V_{tas}}, \quad (3)$$

where  $g$  is gravity. The PI control law generates angular acceleration setpoint  $\alpha_s$  as:

$$\alpha_s = \frac{\bar{V}_{tas}}{V_{tas}} k_{\omega,ff} \omega_s + \left( \frac{\bar{V}_{ias}}{V_{ias}} \right)^2 G_{\omega,PI}(\mathbf{q})(\omega_s - \omega_m), \quad (4)$$

where  $\bar{V}_{tas}$  and  $\bar{V}_{ias}$  are the trim true and indicated airspeeds, respectively,  $k_{\omega,ff}$  is the feedforward proportional gain, and  $\omega_s$  and  $\omega_m$  are the desired and measured body-frame angular velocities, given by

$$\omega_s = \begin{bmatrix} 1 & 0 & \sin\theta \\ 0 & \cos\phi & \sin\phi \cos\theta \\ 0 & -\sin\phi & \cos\phi \cos\theta \end{bmatrix} \begin{bmatrix} \dot{\phi}_s \\ \dot{\theta}_s \\ \dot{\psi}_s \end{bmatrix}. \quad (5)$$

The PI control law is:

$$G_{\omega,PI}(\mathbf{q}) = k_{\omega,P} + \frac{k_{\omega,I}}{\mathbf{q} - 1}, \quad (6)$$

where  $\mathbf{q}$  is the forward-shift operator. The gains  $k_\theta$ ,  $k_\phi$ ,  $k_{\omega,ff}$ ,  $k_{\omega,P}$ , and  $k_{\omega,I}$  constitute 11 variables that must be tuned for flight.

## B. Retrospective Cost Adaptive Control for Fixed-wing Aircraft

Retrospective Cost Adaptive Control [24] is a technique that uses a retrospective cost function to update

the gains of the PID controller recursively. In the present application, we modify Equations 1 and 2 as:

$$\dot{\theta}_s = k_\theta(\theta_s - \theta_m) + u_\theta, \quad (7)$$

$$\dot{\phi}_s = k_\phi(\phi_s - \phi_m) + u_\phi. \quad (8)$$

We modify Equation 4 as :

$$\alpha_s = \frac{\bar{V}_{tas}}{V_{tas}} k_{\omega,ff} \omega_s + \left( \frac{\bar{V}_{ias}}{V_{ias}} \right)^2 G_{\omega,PI}(\mathbf{q})(\omega_s - \omega_m) + u_{\omega,PI}. \quad (9)$$

The control input terms  $u_\theta$ ,  $u_\phi$  and  $u_{\omega,PI}$  are provided by the RCAC controller.

## C. Adaptive Control Law

To understand how RCAC works, consider the example of a SISO PID controller with a feedforward term

$$\begin{aligned}u_k &= K_{p,k}e_{k-1} + K_{i,k}\nu_{k-1} \\ &\quad + K_{d,k}(e_{k-1} - e_{k-2}) + K_{ff,k}r_k,\end{aligned}\quad (10)$$

where  $k \geq 0$ ,  $e_k$  is the error variable,  $r_k$  is the feedforward variable, and

$$\nu_k \stackrel{\text{def}}{=} \sum_{n=0}^k g(e_n) \quad (11)$$

$$= \nu_{k-1} + g(e_{k-1}). \quad (12)$$

A regression synthesizes the control law:

$$u_k = \gamma_k \rho_k, \quad (13)$$

where

$$\gamma_k \stackrel{\text{def}}{=} [e_{k-1} \quad \nu_{k-1} \quad (e_{k-1} - e_{k-2}) \quad r_k], \quad (14)$$

and

$$\rho_k \stackrel{\text{def}}{=} [K_{p,k} \quad K_{i,k} \quad K_{d,k} \quad K_{ff,k}]^T. \quad (15)$$

To determine the controller gains  $\rho_k$ , consider a retrospective performance variable and error model [24]

$$\hat{e}_k(\rho) \stackrel{\text{def}}{=} e_k + \sigma(\gamma_{k-1}\rho - u_{k-1}), \quad (16)$$

and the retrospective cost function  $J_k$

$$\begin{aligned}J_k(\rho) &= \sum_{n=0}^k \hat{e}_n(\rho)^T R_e \hat{e}_n(\rho) \\ &\quad + (\gamma_k \rho)^T R_u (\gamma_k \rho) \\ &\quad + (\rho - \rho_0)^T P_0^{-1} (\rho - \rho_0).\end{aligned}\quad (17)$$

RCAC seeks the minimizer for  $J_k$ , that is

$$\rho_{k+1} \stackrel{\text{def}}{=} \arg \min_{\rho} J_k(\rho). \quad (18)$$

For  $k \geq 0$ ,  $\rho_{k+1}$  is recursively calculated [19]

$$\begin{aligned} \rho_{k+1} = & \rho_k \\ & -\sigma P_{k+1} \gamma_{k-1}^T R_z [e_k + \sigma(\gamma_{k-1} \rho_k - u_{k-1})] \\ & - P_{k+1} \gamma_k^T R_u \gamma_k \rho_k, \end{aligned} \quad (19)$$

where

$$P_{k+1} = P_k - P_k \Gamma_k^T (R_{uz}^{-1} + \Gamma_k P_k \Gamma_k^T)^{-1} \Gamma_k, \quad (20)$$

where

$$\Gamma_k \stackrel{\text{def}}{=} [\sigma \gamma_{k-1} \quad \rho_k]^T, \quad (21)$$

and

$$R_{uz} \stackrel{\text{def}}{=} \begin{bmatrix} R_z & 0 \\ 0 & R_u \end{bmatrix}. \quad (22)$$

The following equation provides the control input

$$u_{k+1} = \gamma_{k+1} \rho_{k+1} \quad (23)$$

The SISO case extends to MIMO through various parameterizations [13]. Here, RCAC modifies the PX4 attitude controller as shown in Equations 7 - 9, where the control inputs  $u_\theta$ ,  $u_\phi$ , and  $u_{\omega, PI}$  are generated for every discrete time step. We refer the reader [24] for additional details of RCAC. The following sections discuss details of applying the stock PX4 and RCAC to flight tests.

## IV. METHODS

Testing the stock and adaptive regimes requires three additional components. They include, space-filling curves at different scales to express flight plans, the stochastic compound failure model, and a measure for comparing the desired and executed flight paths. These are discussed in this section.

### A. Hilbert Curves as Flight Test Patterns

A Hilbert curve [17] is a continuous fractal space-filling curve, typically constructed as a limit of piecewise lines. The Hausdorff dimension of Hilbert curves is two, and its graph is a compact set homeomorphic to the closed unit interval, with Hausdorff dimension 2. The length of the  $n^{\text{th}}$  curve is  $2^n - \frac{1}{2^n}$ , i.e., the size grows exponentially with  $n$ , but each curve is in the unit square [3]. The following pseudo code [2] is an easy example of Hilbert curves:

```
[x, y] ← Hilbert(n)
if n ≤ 0 then
  x ← 0
  y ← 0
else
  [xx, yy] ← Hilbert(n - 1)
```

```
x ← 1/2 * [-1/2 + yy - 1/2 + xx 1/2 + xx 1/2 - yy]
y ← 1/2 * [-1/2 + xx 1/2 + yy 1/2 + yy - 1/2 - xx]
```

**end if**

We designed a flight plan to test various turning frequencies based on Hilbert paths of varying order. We implemented the generation of these curves and used curves of orders 1,2,3 and 4 for each quadrant, respectively, see Figures 6 and 7.

### B. Simulating Compound Failures

The compound failure model tests multiple combinations of failures using a Markov chain. The ground state of *No Failure*: 0 is continued indefinitely until a switch (S/W) on the ground is activated to initiate failures. Turning the switch off reverts the aircraft to *State* - 0 while continuing the flight.

Each transition from the ground state induces a single actuator failure. Although many forms of failure are admissible through our design, we only implemented the corresponding actuator getting stuck (“gummed”) aileron left (AIL-L), right (AIL-R), an elevator (ELE), throttle (THR) or Rudder (Rud). Thus, the corresponding actuator is gummed up once transitioned to these states from the ground state. The aircraft may stay in this state, revert to State 0, or transition to compound failure states that include one more failure. After that transitions can continue through various combinations across states, each additional transitional causing one less or one extra failure, in addition to staying in the same state or returning to the ground state. Certain compound states are never allowed. For example, State 10 in Figure 2, where both the elevator and throttle are stuck, will render the aircraft unrecoverable (depending on the throttle setting). Similarly, for field safety reasons, both ailerons are not failed (though one could still fly with the rudder in some cases). Thus, all the states are in some sense “flyable” while still testing failures.

Our Markov chain simulations used a loop-back probability of 0.3 and a groundstate transition probability of 0.4, distributing the transition edges to valid additional failure states equally amongst the remaining probability. The transitions are discrete in time and activated through their probability every second. Thus, the aircraft must stay in a state for at least one second with a 30% chance of remaining there in the next second, 60% possibility of transitioning to another failure, or a 40% chance of returning to the ground state. In this way, not only is there persistence of a single failure, but various compound and intermittent failures are also triggered. The transition probabilities yield a stationary distribution where all states are reachable.

The stochastic failure model allows for the stochastic realization of adversarial flight conditions. We can obtain performance statistics by simulating an ensemble of such situations, which is more complex than single-perturbation tests (e.g., [24]) for characterizing perfor-

AIL-L	AIL-R	EL E	Thr	Rud	Condition	SW chan8	State
0	0	0	0	0	NO FAIL	0/1	0
1	0	0	0	0	AIL-L Gum	1	1
0	1	0	0	0	AIL-R Gum	1	2
0	0	1	0	0	ELE Gum	1	3
0	0	0	1	0	THR GUM	1	4
0	0	0	0	1	Rud Gum	1	5
1	1	X	X	X	NA	1	6
1	0	1	0	0	Roll-Pitch (airspeed)	1	7
1	0	0	1	0	Roll-Thrust (climb)	1	8
1	0	0	0	1	Roll – Yaw (dangerous)	1	9
X	X	1	1	X	NA	1	10
0	0	1	0	1	Pitch-Yaw (airspeed)	1	11
0	0	0	1	1	Thrust-Yaw (climb)	1	12
1	0	1	0	1	Massive gum up	1	13
1	0	0	1	1	Massive gum up	1	14

Figure 2: Failure states and the corresponding actuator failures. Each row depicts a Boolean condition indicating simulated failure (1) “Gum” of particular actuators or combinations. An *X* indicates that the row (failure) is never simulated (NA). Only if the handheld switch (SW on channel 8 in our setup) is on does the failure simulator proceed.

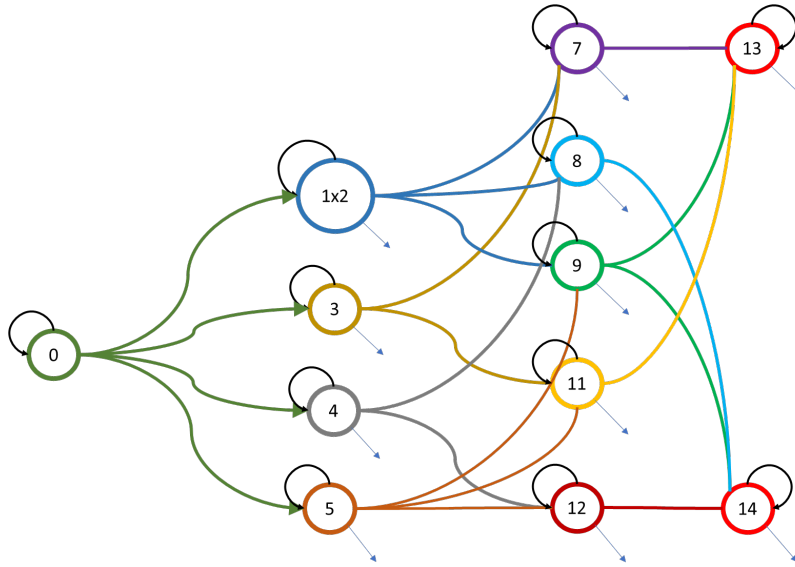


Figure 3: Markov process transition diagram, downward arrows represent edges to the groundstate. The state numbers correspond to the table in Figure 2.

mance. In comparing different control schemes, each method can be subject to the same failure sequence to assess sample-wise and ensemble-wise differences.

### C. Comparing Flight Paths Using Dynamic Time Warping

In analyzing the differences between flight paths, the flight plan, and the flown trajectory, we resample the reference flight plan to the same length as the flown trajectory, saving it at nearly constant time intervals. Since our objective is to assess an ensemble of flight trajectories,

the existence of relative timing differences can lead to the overall inflation of covariance [31]. The Kantorovich-Rubenstein or Wasserstein metric [22], offers a natural approach to dealing with timing errors arriving at features (e.g., sharp turns). Here, to analyze the difference between the aircraft’s performance in regular flight vs. facing a stochastic failure process using Dynamic Time Warping (DTW) [5] between the flight paths. DTW was first proposed within the controls community in the 60s [8] and has since enjoyed broad popularity in comparing discrete signals with index alignment errors. Note that DTW is not a metric, and in that, it differs from the Wasserstein distance. However, it is quick to compute, the values are usually close, and the reference signal (flight plan) is the same. A low DTW distance between the affected and unaffected flight paths represents that the autopilot could maintain course well despite the actuator failures. A high DTW distance implies the opposite. The nominal algorithm for DTW is as follows [1]:

```

DTWfunc( x[1...m], y[1...n]
DTW[i, j] = ∞, ∀i = 1...m, j = 1...n
DTW[0, 0] = 0;
for i=1:m do
  for j=1:n do
    DTW[i, j] = Distance(x[i], y[j]) +
    min(DTW[i - 1, j], DTW[i, j - 1], DTW[i - 1, j - 1])
  end for
end for

```

The function *Distance* is a nominal point-wise Euclidean distance calculation or a metric in Hilbert space. The all-pair calculations incur quadratic costs, and incorporating window/taper functions simplifies it.

## V. IMPLEMENTATION

To implement the control perturbation, we created a new instance of the actuator\_controls channel in the publish-subscribe px4 model. We then added a vehicle command that would tell the simulator or mixer to listen to the new instance of the actuator\_controls topic. Our module then listens to the original actuator\_controls topic and republish it or sends a zero indicating a broken link. Besides creating our module, we had to modify the px4 architecture by altering the simulator module to listen for a command to switch control topic instances. The Pixhawk PX4 (model) we tested with hardware in the loop testing uses two processors to perform flight control. The primary processor handles all of the mathematical computation, and a weaker coprocessor handles output operations and relays sensor information to the primary processor. We initially tried implementing the failure simulation on the IO coprocessor flight controller. Still, this attempt failed because the additional processing of the failure simulation caused the coprocessor to break its real-time condition and crash. The IO coprocessor operates by a serial interface that blind writes into hard-coded memory sections which a critical section reads before be-

ing sent to actuators and other output devices.

One challenge we encountered and could not solve fully was a race condition within the DDS data bus when stopping the failure simulation. Due to the real-time constraints of the system, after instructing the failure simulation process to stop, clock cycles are offered for a limited amount of time before deallocating its memory. This time is, unfortunately, faster than the update rate of the simulator, which waits for a signal to switch back to the original control signal instance only after attempting to read from the deallocated phony control signal buffer. That meant we could not stop the failure simulation process once it started. We could, however, command it not to modify the control inputs it parses and pass them along to the mixer unmodified, effectively disabling the purpose of the process.

## VI. EXPERIMENTS

The PX4 autopilot is well-tuned for many hobby UAS. We calculated these gains for the aircraft under consideration 1 through extensive flight testing starting from readily available gains for similar aircraft. For RCAC, we performed several flight tests. We checked whether the parameter led to unstable flight in assisted mode with random flight-stick inputs for each controlled attitude variable. In many cases, the onset of instability occurred a considerable time after the stick perturbation. Therefore, we set nominal values, which may slow the gain adaptation and be sub-optimal. Table I lists the settings we used.

PTCH	P0	1
PTCH	RU	0.001
PITCH RATE	P0	1e-4
PITCH RATE	RU	0.1
ROLL	P0	1
ROLL	RU	0.001
ROL RATE	P0	1e-4
ROLL RATE	RU	0.1
YAW RATE	P0	1e-4
YAW RATE	RU	0.1

Table I: Nominal RCAC (hyper) parameters. The mixing variable  $\alpha$  is to 1 (or 0.5).

For the standard PX4 PID-based autopilot, we ran eight trials of the stochastic adversarial actuator failure process, two of which resulted in a crash. For an experimental Retrospective Cost Adaptive Control (RCAC) algorithm, we ran 15 trials, 3 of which resulted in a crash. As a baseline, we also ran several clean flights of the PX4 PID controller and saw they had an average DTW metric of 133 meters with a standard deviation of 47 meters. We then did the same for the RCAC autopilot and saw that they had an average self-similarity under the DTW metric of 136 meters with a standard deviation of 35 meters.

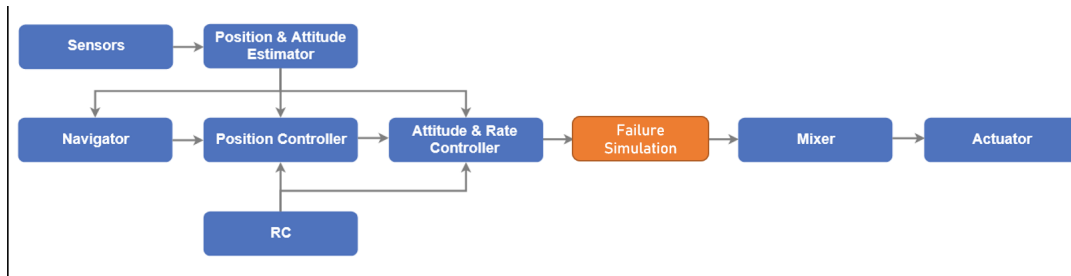


Figure 4: Modified PX4 architecture showing the failure injection module (in orange).

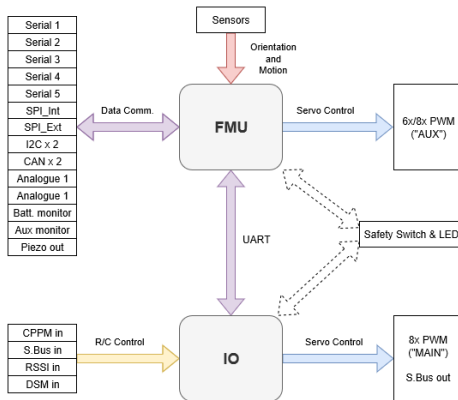


Figure 5: The PX4 implementation [6] on PixHawk [4] splits the computation between two processors. Failure streams were re-implemented on FMU because the IO processor was weaker and could not sustain the computation.

The mean distance between perturbed and ideal flight paths for the standard autopilot is 595 meters, with a standard deviation of 154 meters. The mean distance between perturbed and ideal flight paths for the RCAC autopilot was 610 meters, with a standard deviation of 163 meters. Figure 8 shows that the variance and mean of the failure-induced paths for RCAC are slightly worse in the clean condition where they are slightly better in the clean condition. Additional, possibly dynamic tuning of hyper-parameters is most likely warranted.

## VII. CONCLUSIONS AND FUTURE WORK

This paper considers transient singleton, compound, and cascading actuator failure scenarios and tests the performance of a stock autopilot PX4 (v1.10) simulation for Holybro Pixhawk (FMUv5) hardware and fixed-wing aircraft. In actual flight experiments we have conducted elsewhere, multiple failures often cascade. For example, transient spikes in electrical load can trigger losses anywhere in the system. The PX4 autopilot, like others, is often tuned for the aircraft, and considerable attention is

devoted to this effort before commencing flight missions. The case for extending RCAC-like adaptive control from tuning degraded gains to failure streams emerging in well-tuned autopilots is interesting and essential. The operational setting is of a tuned autopilot with the RCAC as “safety” that would compensate for the transient failure stream.

In this paper, a Markov chain simulates failures with a stationary distribution that reaches all clean and adverse modes. The Markov chain is designed not to cause total catastrophic failure of the aircraft. Simulated Hilbert curves are flight paths for testing PX4 and PX4-RCAC, with mixing parameter  $\alpha = 1$ . The PX4 flight parameters were determined for the model aircraft through flight testing and set in simulations. We selected RCAC hyper-parameters that led to stable flight over long duration for the same model aircraft. DTW was used to compare resampled flight plans and simulated flight paths to account for timing-error artifacts between ensemble simulations. The ensemble simulations calculate the mean position error and the error variance. Under clean configurations, RCAC slightly outperforms PX4, but under the hostile regime, it under performs. Additional, possibly dynamic, hyper-parameter tuning may be required to deal with intermittent failure streams. With the extra work, we will implement this in actual flight tests in the future. We also anticipate learning the Markov chain using flight logs gleaned from the PX4 community.

## VIII. CONTRIBUTIONS AND ACKNOWLEDGMENT

Corresponding Author: Thelonious Cooper (*theloni@mit.edu*). Thelonious Cooper wrote code and performed the experiments, Sai Ravela developed the transition tables, and Erina Yamaguchi reported the original Hilbert path code. Cooper and Ravela drafted and edited the paper. We thank Prof. Ankit Goel, Jyonghoon Lee, Juan Augusto Paredes, John Spencer, and Prof. Dennis Bernstein for their support and collaboration. We are grateful for funding from ONR (N00014-19-1-2273) and the MIT Weather Extreme and CREWSNET Climate Grand Challenge projects.

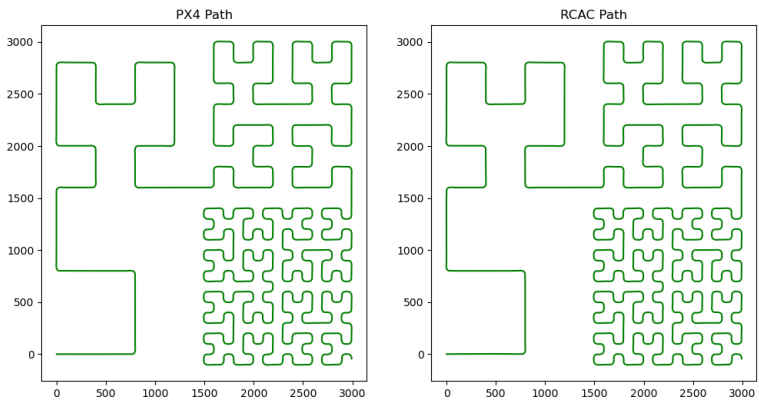


Figure 6: Examples of Nominal Flight Paths for PX4 (left) and RCAC (right).

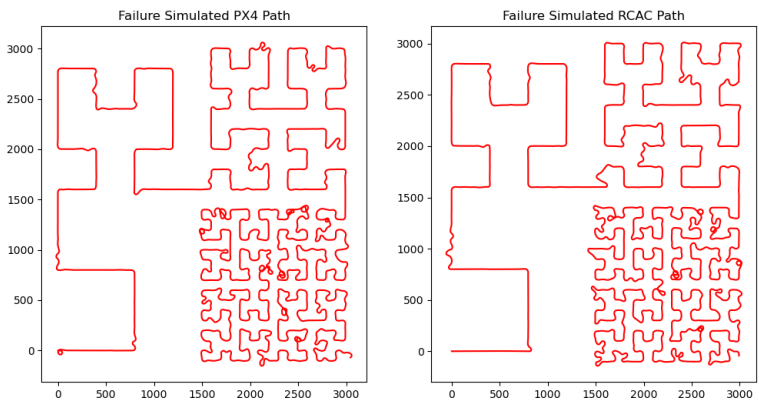


Figure 7: Examples of Failure Simulated Flight Paths for PX4 (left) and RCAC (right).

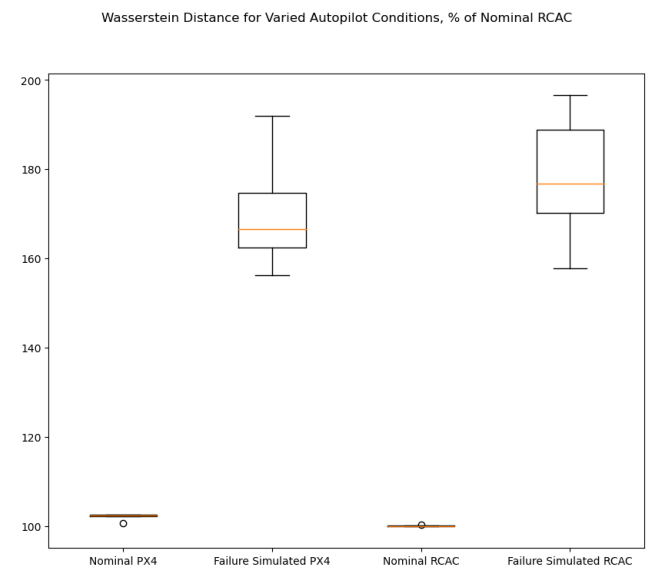


Figure 8: Boxplot of DTW distances for nominal (clean) and failure simulated (adversarial) flight conditions.

[1] Dynamic time warping - Wikipedia — en.wikipedia.org. [https://en.wikipedia.org/wiki/Dynamic\\_time\\_](https://en.wikipedia.org/wiki/Dynamic_time_)



- warping. [Accessed 14-May-2023].
- [2] Hilbert Curve — mathworks.com. <https://www.mathworks.com/matlabcentral/fileexchange/4646-hilbert-curve>. [Accessed 14-May-2023].
  - [3] Hilbert curve - Wikipedia — en.wikipedia.org. [https://en.wikipedia.org/wiki/Hilbert\\_curve](https://en.wikipedia.org/wiki/Hilbert_curve). [Accessed 14-May-2023].
  - [4] Holybro Pixhawk 4 (FMUv5): PX4 User Guide. [https://docs.px4.io/v1.11/en/flight\\_controller/pixhawk4.html](https://docs.px4.io/v1.11/en/flight_controller/pixhawk4.html). [Accessed 14-May-2023].
  - [5] *Dynamic Time Warping*, pages 69–84. Springer Berlin Heidelberg, Berlin, Heidelberg, 2007.
  - [6] PX4 Reference Flight Controller Design, PX4 User Guide. [https://docs.px4.io/main/en/hardware/reference\\_design.html](https://docs.px4.io/main/en/hardware/reference_design.html), 2022. [Accessed 14-May-2023].
  - [7] M.E. Argyle and R.W. Beard. Nonlinear total energy control for the longitudinal dynamics of an aircraft. In *2016 American Control Conference (ACC)*, page 6741–6746.
  - [8] R. Bellman and R. Kalaba. On adaptive control processes. *IRE Transactions on Automatic Control*, 4(2):1–9, 1959.
  - [9] K. Bruce, J. Kelly, and J. Person. Nasa b737 flight test results of the total energy control system. In *Astrodynamics Conference*, page 2143.
  - [10] Thelonious Cooper, Erina Yamaguchi, and Sai Ravela. ESSG (MIT) PX4 Failure Simulator Flight Stack. <https://github.com/theloni-monk/PX4-Autopilot-ESSG-FWFA>, 2022. [Accessed 14-May-2023].
  - [11] L. Faleiro and A. Lambregts. Analysis and tuning of a total energy control system control law using eigenstructure assignment. *Aerospace science and technology*, 3(3):127–140,.
  - [12] M. Fu, Z. Yu, and Y. Zhang. Adaptive fault-tolerant control of fixedwing uav under actuator saturation and state constraints. In *2021 International Conference on Unmanned Aircraft Systems (ICUAS)*, page 47–52.
  - [13] A. Goel, S.A.U. Islam, and D.S. Bernstein. Adaptive control of mimo systems using sparsely parameterized controllers. In *2020 American Control Conference (ACC)*, page 5340–5345.
  - [14] A. Goel, J.A. Paredes, H. Dadhaniya, S.A.U. Islam, A.M. Salim, S. Ravela, and D. Bernstein. Experimental implementation of an adaptive digital autopilot. In *2021 American Control Conference (ACC)*, page 3737–3742.
  - [15] Ankit Goel, Abdulazeez Mohammed Salim, Ahmad Ansari, Sai Ravela, and Dennis Bernstein. Adaptive digital pid control of a quadcopter with unknown dynamics. *arXiv:2006.00416*, 2020.
  - [16] Siyang Gong, Shengwei Meng, Benkuan Wang, and Datong Liu. Hardware-in-the-loop simulation of uav for fault injection. In *2019 Prognostics and System Health Management Conference (PHM-Qingdao)*, pages 1–6, 2019.
  - [17] D. Hilbert. Über die stetige abbildung einer linie auf ein flächenstück. *Mathematische Annalen*, (38):459–460, 1891.
  - [18] S. Hirano, K. Uchiyama, and K. Masuda. Controller design using backstepping algorithm for fixed-wing uav with thrust vectoring system. In *2019 International Conference on Unmanned Aircraft Systems (ICUAS)*, page 1084–1088. IEEE.
  - [19] S.A.U. Islam and D.S. Bernstein. Recursive least squares for real-time implementation. *IEEE Control Systems Magazine*, 39(3):82–85,.
  - [20] Saurabh Jha, Subho S. Banerjee, James Cyriac, Zbigniew T. Kalbarczyk, and Ravishankar K. Iyer. Avfi: Fault injection for autonomous vehicles. In *2018 48th Annual IEEE/IFIP International Conference on Dependable Systems and Networks Workshops (DSN-W)*, pages 55–56, 2018.
  - [21] M. Kamaldar, S.A.U. Islam, S. Sanjeevini, A. Goel, J.B. Hoagg, and D.S. Bernstein. Adaptive digital pid control of first-order-lag plus-dead-time dynamics with sensor, actuator, and feedback nonlinearities. *Advanced Control for Applications*, 1(1):20,.
  - [22] L. V. Kantorovich. Mathematical methods of organizing and planning production. *Management Science*, 6(4):366–422, 1960.
  - [23] A.A. Lambregts. Tecs generalized airplane control system design—an update. In *Advances in Aerospace Guidance, Navigation and Control*, page 503–534. Springer.
  - [24] Joonghyun Lee, John Spencer, Juan Augusto Paredes, Sai Ravela, Dennis S. Bernstein, and Ankit Goel. An adaptive digital autopilot for fixed-wing aircraft with actuator faults. *arXiv:2110.11390*, 2021.
  - [25] Lorenz Meier, Dominik Honegger, and Marc Pollefeys. Px4: A node-based multithreaded open source robotics framework for deeply embedded platforms. In *2015 IEEE International Conference on Robotics and Automation (ICRA)*, pages 6235–6240, 2015.
  - [26] N. Nguyen, K. Krishnakumar, J. Kaneshige, and P. Nespeca. Dynamics and adaptive control for stability recovery of damaged asymmetric aircraft. In *AIAA Guidance, navigation, and control Conference and Exhibit*, page 6049.
  - [27] S. Park, J. Deyst, and J. How. A new nonlinear guidance logic for trajectory tracking. In *AIAA guidance, navigation, and control conference and exhibit*, page 4900.
  - [28] F. Prochazka, S. Krüger, G. Stomberg, and M. Bauer. Development of a hardware-in-the-loop demonstrator for the validation of fault-tolerant control methods for a hybrid UAV. *CEAS Aeronautical Journal*, 12(3):549–558, August 2021.
  - [29] Y. Rahman, A. Xie, and D.S. Bernstein. Retrospective cost adaptive control: Pole placement, frequency response, and connections with lqg control. *IEEE Control System Magazine*, 37(5):28–69,.
  - [30] Sai Ravela. Mapping coherent atmospheric structures with small unmanned aircraft systems. In *AIAA Infotech@Aerospace (I@A) Conference*, pages 1–11, 2013.
  - [31] Sai Ravela. Statistical Inference for Coherent Fluids. *LNCS*, 8964:121–133, 2015.
  - [32] Sai Ravela. *Tractable Non-Gaussian Representations in Dynamic Data Driven Coherent Fluid Mapping*, pages 29–46. Springer International Publishing, Cham, 2018.
  - [33] J. Spencer, J. Lee, J.A. Paredes, A. Goel, and D. Bernstein. An adaptive pid autotuner for multicopters with experimental results. *arXiv:2109.12797*.
  - [34] Margaret Trautner, Gabriel Margolis, and Sai Ravela. Informative neural ensemble kalman learning. *arXiv:2008.09915*, 2020.
  - [35] Jiayun Wen, Hongxia Ji, Honglun Wang, Menghua Zhang, Dawei Li, and Jianfa Wu. Design of a real-time uav fault injection simulation system. In *2019 IEEE International Conference on Unmanned Systems (ICUS)*,

- pages 767–772, 2019.
- [36] J. Xiong, Y. Yang, Z. Cheng, L. Liu, Y. Wang, and H. Fan. Observer like model reference adaptive augmenting based fixed-wing uav control. In *2020 39th Chinese Control Conference (CCC)*, page 6804–6809.
- [37] Z. Yu, H. Badihi, Y. Zhang, Y. Ma, B. Jiang, and C.-Y. Su. Fractional order sliding-mode fault-tolerant neural adaptive control of fixed-wing uav with prescribed tracking performance. In *2020 2nd International Conference on Industrial Artificial Intelligence (IAI)*, page 1–6.